BIODEGRADATION OF POROUS CALCIUM PHOSPHATE SCAFFOLDS IN AN ECTOPIC BONE FORMATION MODEL STUDIED BY X-RAY COMPUTED MICROTOMOGRAPHY

V.S. Komlev[1,2], M. Mastrogiacomo[1], R.C. Pereira[1,5], F. Peyrin[3,], F. Rustichelli[4], and R. Cancedda[1]*

[1] Istituto Nazionale per la Ricerca sul Cancro and Dipartimento di Oncologia, Biologia e Genetica dell'Universita' di Genova, Genova, Italy

[2] A.A. Baikov Institute of Metallurgy and Materials Science, Russian Academy of Sciences, Moscow, Russia

[3] European Synchrotron Radiation Facility, 38043 Grenoble Cedex, France and CREATIS-LRMN Inserm U630; UMR CNRS 5220; INSA Lyon; Université de Lyon; 69621 Villeurbanne Cedex, France

[4] Section of Physical Sciences, Department S.A.I.F.E.T., Polytechnic University of Marche, Ancona, Italy and Istituto Nazionale Biostrutture e Biosistemi (INBB) - CNISM - Matec, Ancona, Italy

[5] Department of Polymer Engineering, University of Minho, Campus de Gualtar and the Institute for Biotechnology and Bioengineering, PT Government Associated Laboratory, Braga, Portugal

Abstract

Three types of ceramic scaffolds with different composition and structure [namely synthetic 100% hydroxyapatite (HA; Engipore), synthetic calcium phosphate multiphase biomaterial containing 67% silicon stabilized tricalcium phosphate (Si-TCP; Skelite™) and natural bone mineral derived scaffolds (Bio-oss®)] were seeded with mesenchymal stem cells (MSC) and ectopically implanted for 8 and 16 weeks in immunodeficient mice. X-ray synchrotron radiation microtomography was used to derive 3D structural information on the same scaffolds both before and after implantation. Meaningful images and morphometric parameters such as scaffold and bone volume fraction, mean thickness and thickness distribution of the different phases as a function of the implantation time, were obtained. The used imaging algorithms allowed a direct comparison and registration of the 3D structure before and after implantation of the same sub-volume of a given scaffold. In this way it was possible to directly monitor the tissue engineered bone growth and the complete or partial degradation of the scaffold.

Further, the detailed kinetics studies on Skelite™ scaffolds implanted for different length of times from 3 days to 24 weeks, revealed in the X-ray absorption histograms two separate peaks associated to HA and TCP. It was therefore possible to observe that the progressive degradation of the Skelite™ scaffolds was mainly due to the resorption of TCP. The different saturation times in the tissue engineered bone growth and in the TCP resorption confirmed that the bone growth was not limited the scaffold regions that were resorbed but continued in the inward direction with respect to the pore surface.

Keywords: Biodegradation, porous calcium phosphate scaffolds, X-ray computed microtomography, registration.

*Address for correspondence:
Ranieri Cancedda
Istituto Nazionale per la Ricerca sul Cancro,
Largo R. Benzi, 10, 16132 Genova,-Italy
Telephone Number: +39-0105737398
FAX Number: +39-0105737257
E-mail: ranieri.cancedda@unige.it

Introduction

In recent years, synthetic and natural porous ceramic materials have been widely used as scaffolds in bone tissue engineering (Anselme *et al.,* 1999; Hench and Polak, 2002; Cancedda *et al.*, 2003). Major requirements for such materials are biocompatibility, porosity and a biodegradation rate corresponding to the one of bone formation upon replacement of the scaffold by the new bone tissue (Langer and Vacanti, 1993). As the new bone tissue incorporates the scaffold material, the scaffold itself should be biodegradable either through cellular events or as a result of the surrounding environment (Mastrogiacomo *et al.*, 2007). However, the exact mechanism of the scaffold biodegradation has been only partially clarified and the results from the different studies are often contradictory.

Histological observations from animal studies and human biopsies showed that calcium phosphate and hydroxyapatite (HA) based materials, such as bioactive glass and tricalcium phosphate (TCP) degrade mainly by physicochemical dissolution with osteoclasts playing only a minor role (Tadjoedin *et al.*, 2000; Suba *et al.*, 2006). This finding is in agreement with the results obtained by Knabe *et al.* (2008), who examined human biopsies and specimens from a sheep study. In these investigations, undecalcified histological sections were stained for tartrate-resistant acid phosphatase activity to reveal the possible presence of cells with osteoclastic activity close to the calcium phosphate bone substitute materials. On the contrary, other authors reported that scaffold biodegradation occurred mainly as result of an osteoclastic activity (Schepers *et al.*, 1991; Mastrogiacomo *et al.*, 2007). The latter mechanism of biodegradation is to be preferred (Schenk, 1991; Rumpel *et al.*, 2006), because mimicry of the physiological bone resorption process should create optimal surfaces for colonization by osteoblasts and vascular tissue.

In the literature, different opinions exist on the biodegradation of the natural bone derived mineral scaffolds, such as Bio-Oss®, but the prevalent view is that they can be resorbed (Rumpel *et al.*, 2006). Duda and Pajak (2004), amongst others, have observed Bio-Oss® remnants in patients even several years after

implantation. Implantations performed in dog cranial bones (Merkx *et al.*, 1997) could not demonstrate significant biodegradation after several months, although the biomaterial could be resorbed by osteoclast-like cells (Merkx *et al.*, 1999). Indeed, a recent human study (Zaffe *et al.*, 2005) reports biodegradation of these biomaterials by osteoclasts.

The reason for such apparent discrepancies may lie in the used models and/or the adopted techniques. In general terms, traditional histological analyses may be scored or graded based on degree of tissue necrosis/degeneration, fibrosis, and types and amounts of inflammatory and foreign body giant cells present. It is clear that such tests do not fully measure biodegradation ability and do not allow the understanding of the underlying mechanisms. Fluid extracts from scaffolds may be used to determine the presence of an acute biological reactivity and of possible degradation compounds (Bumgardner *et al.*, 2004). Attempts have been performed to study resorbability based on combining standard radiographic image analysis and histology (Giannoni *et al.*, 2008). However, the results are clearly unsatisfactory, although consistent with the other applied techniques, and a need for improvement exists. In this context the three-dimensional (3D) nondestructive X-ray computed microtomography (microCT) may contribute to a better understanding of the biodegradation processes and therefore, to a better fulfillment of the tissue engineering needs for the development of the future generation biomaterials (Komlev *et al.*, 2006; Cancedda *et al.*, 2007). Several publications are dealing with studies by microCT of the biodegradation of the implanted porous scaffolds (Papadimitropoulos *et al.*, 2007; Renghini *et al.*, 2009). All these studies compared in different scaffolds the percentage of the total sample volume fracture or the thickness of the investigated biomaterials either before (control) or after implantation. At most, different sub-volumes of the same scaffolds before and after implantation were analyzed. Therefore, scaffold degradation rate and mechanism were not exactly monitored by these approaches.

In fact, microCT images of the same scaffold volume acquired at different times (before and after implantation) should be combined to more satisfactorily study the scaffold biodegradation. However, structures are likely to have changed their positions between the acquisitions due to a number of reasons, and combining the images could be a very difficult experimental task. Indeed, combining these types of images requires their geometric warping so that corresponding image structures correctly align – image registration. Such techniques have for instance been applied to the evaluation of bone loss in ovariectomized animal models (Waarsing *et al.*, 2006; Klinck *et al.*, 2008). At the present, there are a number of different kinds of registration techniques (Brown 1992; van den Elsen *et al.*, 1993; Modersitzki, 2004; Schmitt *et al.*, 2007) for different registration problems, in particular for the alignment of images of serial sections. This includes e.g., rigid, affine and elastic registration. Rigid and affine transformations are easy to be unequivocally formulated in simple mathematical terms and need only very few parameters to be adjusted for registration, namely: translations, rotations, scaling factors, and skewing factors. However, significant deviations may remain after rigid/affine registrations. To compensate for those, elastic registration needs to be applied. Contrary to its rigid/affine counterparts, elastic registration has not yet become a standard technique that is used on a routine basis, the reason being that elastic registration is much more difficult to achieve and, as of yet, no generally accepted solution is available (Hamisch *et al.*, 2006). These methods will help with the registration of highly disparate modalities that provide insufficient image structures. On the other hand, none of them were applied to investigate biodegradation of the scaffolds.

In this work, to investigate scaffold degradation, a well-established model of ectopic bone formation was adopted in which bone marrow-derived mesenchymal stem cells (MSC) were loaded onto different porous scaffolds and subcutaneously implanted in immunodeficient mice. Scaffolds implanted in the mice for different lengths of time were analyzed by microCT using registration of several series of images.

Materials and Methods

Porous ceramic scaffolds and tissue engineering constructs

Marrow aspirates were obtained from the iliac crest of sheep as part of a protocol approved by the competent ethics authority. Detailed protocol for bone marrow-derived mesenchymal stem cells (MSC) expansion *in vitro* and histological protocols have been described elsewhere (Muraglia *et al.*, 1998). Briefly, the cell-nucleated fraction of 20 mL bone marrow aspirate was suspended in Coon's modified Ham's F12 medium supplemented with 10% fetal calf serum, human recombinant fibroblast growth factor 2 (1 ng/mL), and antibiotics, and plated at a density of 1×10^6 cells/cm^2. Medium was changed twice a week. When culture dishes were nearly confluent (passage 0), MSC were detached with trypsin-EDTA and 5×10^5 cells were replated in 100 mm dishes (passage 1). At the next subconfluence, MSC were detached and used for implants.

Three types of bioceramic scaffolds were considered, namely synthetic 100 % hydroxyapatite (HA; Engipore), synthetic calcium phosphate multiphase biomaterial containing 67% silicon stabilized tricalcium phosphate (Si-TCP; Skelite™) and natural bone mineral derived scaffold (Bio-Oss®). All scaffolds were small cubes with a dimension of about 4×4×4mm. Bioceramic/MSC composites were implanted subcutaneously on the back of the mice (up to four implants for each animal). Mice were sacrificed at different lengths of time after implantation, and the harvested samples were fixed in paraformaldehyde (PFA 4% in phosphate buffered saline, PBS) for 2 h at 4°C.

Image acquisition: synchrotron radiation microCT

MicroCT experiments were performed using synchrotron radiation at the ID19 beam line of the European Synchrotron Radiation Facility (ESRF) in Grenoble, France. The acquisition setup is based on three-dimensional (3D) parallel tomography previously described (Salome

et al., 1999). Briefly, the transmitted intensity was recorded by a two-dimensional (2D) detector, which consists of a Gadox scintillator (an X-ray-to-visible light converter), light optics for magnification of the image, and a FReLoN CCD camera developed at the ESRF. The camera has 14-bit dynamic range and a 2048×2048 pixel chip. In our experiments, the pixel size was fixed at 4.91 μm, thus yielding a field view of 6 mm. The sample-to-detector distance was fixed at 15 mm and a 27 keV beam energy was found to provide suitable contrast as reported in (Komlev *et al.*, 2006). The exposure time was 3 s per projection. For each sample, 1100 radiographic images (or projections) with 2048×2048 pixels were acquired at different angles of view, ranging from 0 to 180°.

Image reconstruction for microCT

After tomographic acquisitions, 3D images were reconstructed from the series of 2D projections using a 3D filtered back projection algorithm implemented at ESRF (Salome *et al.*, 1999). A volume of about 800^3 voxels was reconstructed, yielding a voxel with a 4.91 μm size in the three directions of space.

3D visualization and parameters quantification

Direct volume rendering (DVR) methods were selected to map elements directly into screen space without using geometric primitives as an intermediate representation. To this end, the commercial software VG Studio MAX 1.2.1 (Volume Graphics GmbH, Heidelberg, Germany) was used to produce 3D images, which efficiently implemented various DVR methods, especially with large volume datasets.

Volume segmentations

An automated multi-threshold segmentation method based on (Otsu *et al.*, 1979) was used to highlight and separate the different phases (scaffold, bone) from background. More precisely, after separation of the different phases by a multi-thresholding procedure of post implanted samples, each of the histograms was partitioned in equal zones according to (Papadimitropoulos *et al.*, 2007).

Image analysis tools derived from mathematical morphology are often used to process images (Matheron, 1975; Serra, 1982). The basic morphological operations are erosion and dilation. Dilation, in general, causes objects to dilate or grow in size; erosion causes objects to shrink. The amount and the way that they grow or shrink depend upon the choice of the structured element. The opening operation is somewhat like erosion in that it tends to remove some of the foreground (bright) pixels from the edges of regions of foreground pixels. On the other hand, "closing" is similar in some ways to dilation but it is less destructive of the original boundary shape (Iyer and Sinha, 2006). Therefore, the mathematical morphology operator "closing" was applied to enlarge the boundaries of foreground regions, shrink background holes and isolated points.

Extraction of quantitative parameters

The 3D data volumes produced by the image reconstruction process were used in order to quantify the parameters, which characterize the structures of the scaffold and of the new bone. Once the different phases were segmented, volumes of the phases itself (bone volume and scaffold volume) were easily calculated counting the voxels in the specified segmented data range. Morphometric parameters, such as new bone and scaffold thicknesses, were evaluated according to (Dougherty and Kunzelmann, 2007), where the mean thickness and its distribution were calculated in a direct way and independently of an assumed structural model. Briefly, the computation of the thickness value was defined as the average of the local thickness at each voxel representing a given phase (new bone and scaffold). The volume-based local thickness for a point in a phase was defined as the maximal diameter of a sphere, which satisfies simultaneously the conditions: (a) the sphere encloses the point and (b) the sphere is entirely bounded within the phase.

Volume registration

In the first approach we applied well-known affine linear registration that is based on gray level intensities. Volume registration was used in Java as a plugin for free open software ImageJ (http://rsbweb.nih.gov). It can be performed by automatic 3D registration either on the whole volume or on the selected subvolume. Volume registration using the whole volume can be too lengthy to be practical for moderately sized images. Therefore, only the selected 3D subvolumes after segmentations (see Volume segmentation) were registered. The value of the similarity function during optimization was applied too. Similarity functions include correlation coefficient, sum of absolute differences, and mutual information. Transformations include various types of affine (non-warping) operations. The optimization algorithms include Powell's algorithm, a parabolic fit to random points, simulated annealing, or no operation (useful for plotting). Interpolation methods include nearest neighbor, tri-linear and a random jitter. Similarity functions can be summarized as follow: the correlation coefficient is defined as $E\{(f-m_f)*(g-m_g)\}/(E\{(f-m_f)^2\}*E\{(g-m_g)^2\})^{1/2}$, where f and g are the pixel values of two images (F and G), E{} is the average over the pixels in the image, and m_f and m_g are the respective mean values. The correlation coefficient is just a cross correlation normalized for the power in the images. The sum of absolute differences is defined as $1-\text{sum}\{|(f-m_f)-(g-m_g)|\}/\text{sum}\{|f-m_f|+|g-m_g|\}$, where sum{} is the sum over the pixels in the image. Both the correlation coefficient and the sum of absolute differences assume that the two images are on the same scale. White objects in F correspond to white objects in G, and black objects in F correspond to black objects in G. These two similarity functions are most appropriate for aligning images from the same modality, e.g. microCT. More information can be found at http://rsbweb.nih.gov.

However, after affine linear registration, images are affected by local nonlinear deformations that need to be reduced by the nonlinear approach elastic registration (Schmitt *et al.*, 2007). Therefore, a local nonlinear technique like elastic registration is an inevitable procedure for a consequent final alignment of microCT images. To this purpose, an ImageJ plugin that allows the simultaneous

Table 1. Histomorphometric data for scaffolds before implant.

	PoreD (microns)	PoreV (%)	S.Th (microns)
Engipore	430±202	79±5	101±42
Skelite™	655±354	75±5	215±175
Bio-Oss®	455±155	81±3	141±47

S.Th = scaffold mean thickness; PoreV = total volume of the pores; PoreD = pore diameter.

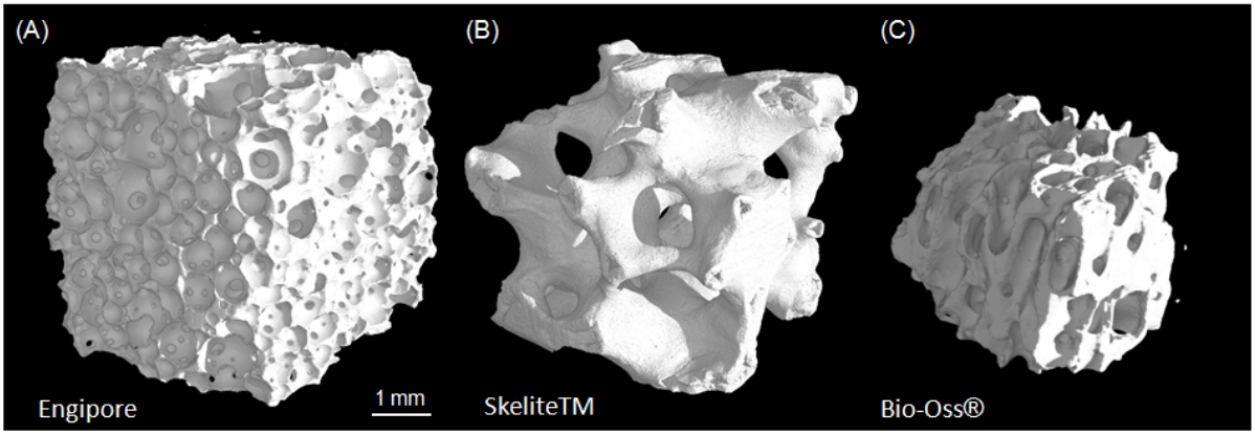

Fig. 1: 3D display of different scaffolds before implantation: **(A)** Engipore (hydroxyapatite) produced by FinCeramica, Faenza, Italy; **(B)** Skelite™ (silicon-stabilized tricalcium phosphate) produced by Millenium Biologics Kingston, Ontario, Canada; **(C)** Bio-Oss® (natural bone mineral) produced by Geistlich Pharma AG, Wolhusen, Switzerland.

registration of two images based on elastic deformations represented by B-splines was used (Sánchez Sorzano *et al.*, 2005). B-splines are piecewise-polynomial bases with a low computational cost, which makes them very attractive. Because their approximation properties are optimal in a mathematically well-defined sense, they are extremely useful to model many functions; in particular, the deformation field can be viewed as a set of several functions (one per coordinate) which in turn are modeled by a linear sum of weighted and shifted B-splines. The set of weights, which are called the B-spline coefficients, fully characterize the transformation (Sánchez Sorzano *et al.*, 2005).

Finally, synchronization should be used. Synchronization may be interactive or partially or fully automatic with help of a fusion algorithm that is described elsewhere (Stokking *et al.*, 2003). We adopted the full fusion automatic algorithm. The exact synchronization of data sets provides capacity for image fusion with superimposition of both sets of imaging data in one image data set for further treatment.

Results

To investigate scaffold biodegradation occurring *in vivo*, microCT acquisitions were performed on the same scaffolds prior and after cell seeding and implantation thus enabling *in situ* comparative studies. Small cubes of three different scaffolds (Engipore (hydroxyapatite), Skelite™ (silicon-stabilized tricalcium phosphate) and Bio-Oss® (natural bone mineral)) were imaged (Fig. 1) before cell seeding and implantation in immunodeficient mice for 8 and 16 weeks, respectively. Significant differences existed in the internal microarchitecture of the three scaffolds. Histomorphometric data for the scaffolds before implantation are reported in Table 1.

When microCT data of the scaffolds obtained both before and after implantation were considered, we first compared the thickness distributions of the scaffold walls (Fig. 2 panels A-C). Examples of a central virtual slice through the 3D structure of each sample showing the local wall thickness map before and after implantation, are shown in Fig. 2 (panels A1-C2). From these distributions a significant degradation in the implanted scaffold could be observed only in Skelite™. In Engipore and Bio-Oss® no and a little decrease, respectively, of the scaffold wall thickness were detected. To illustrate the quality of the data an example of data treatment for non- (Engipore) and resorbable (Skelite™) scaffolds is presented in Fig. 3. Our obtained results are in agreement with those reported in (Papadimitropoulos *et al.*, 2007; Peyrin *et al.*, 2007; Dougherty and Kunzelmann, 2007).

Volume registration was used to register images of the same scaffolds before and after implantation as described in the Materials and Methods section. The 3D displays of subvolumes of all three scaffolds before implantation are shown in Fig. 4 (panels A0-C0). In order to have a pictorial view and a better basis for the interpretation of the registered images, in Fig. 4 (panels A1-C1) we also present

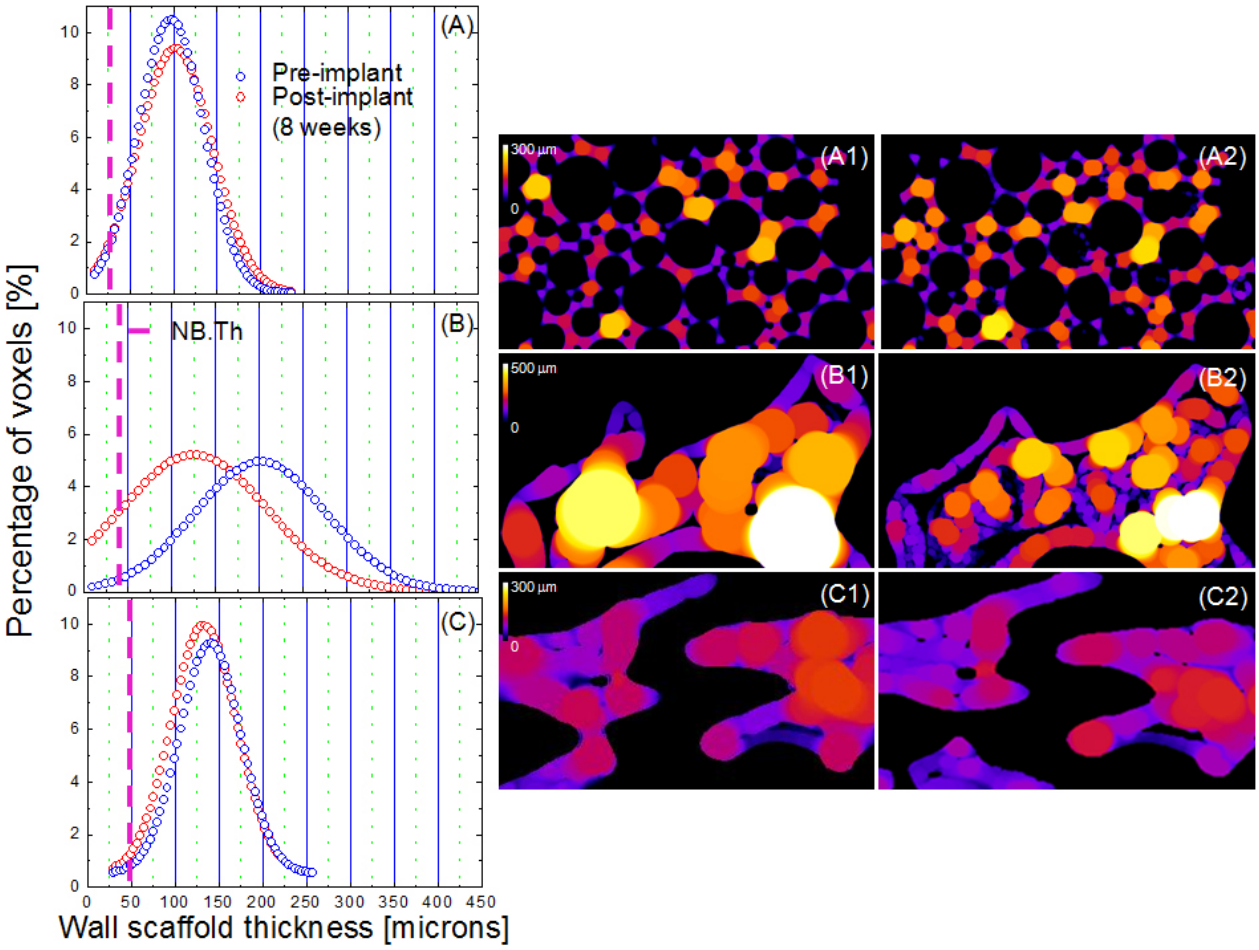

Fig. 2: Histograms of the distribution of wall thickness before and after scaffold implantation: **(A)** Engipore (hydroxyapatite); **(B)** Skelite™ (silicon-stabilized tricalcium phosphate); **(C)** Bio-Oss® (natural bone mineral). NbTh = New Bone Thickness. **(A1-C2)** Examples of central slices through the samples within the 3D local wall thickness map before **(A1-C1)** and after implantation **(A2-C2)**. The thickness in each point is coded according to the color map included in panels **A1, B1, C1**.

images of the bone tissue-engineered constructs of the same sub-volumes at 8 weeks after implantation in mice. Scaffold material (white) and the new bone (pink) are clearly visible. The 3D displays of the registered pre- and post implanted images are shown in panels A2-C2: blue volumes indicate portions of scaffolds present in the pre-implantation sample and to void volumes after implantation and correspond to completely resorbed scaffolds. Yellow volumes indicate original scaffold volumes in which after implantation a reduction of the sample density was observed and could correspond to partially resorbed scaffold, or to deposited bone with a higher density (bone with a particular high mineral content), or a combination of the two (bone deposition in a partially resorbed scaffold). Also this type of analysis confirmed that a significant scaffold biodegradation after 8 weeks implantation occurred only in the Skelite™ sample, while a minimal biodegradation was observed in the Bio-Oss® and none in the Engipore samples. Based on these findings, the scaffold degradation in the tissue engineered implanted constructs was investigated after 16 weeks implantation only for the Skelite™.

3D displays of registered images of pre- and post implantation Skelite™ samples implanted for 8 (A) and 16 (B) weeks are presented in Fig. 5 (panels A-B), respectively. As in the registered images of Fig. 4 (panel B2) blue and yellow correspond to totally and partially resorbed scaffold, respectively. The volume percentage distribution of the different phases is presented in panels A1 and B1. An increase in the percentage of the resorbed scaffold was observed with the increased implantation time.

To better investigate the transition zone between Skelite™ scaffold and bone where an overlap could exist between newly deposited bone and partially resorbed scaffold, as well as to depict spatial correlations between the different phases, different color hues were applied to the volume histograms (Papadimitropoulos *et al.*, 2007). In Fig.6, after separation of the different phases by a multi-thresholding procedure (see Materials and Methods), each of the histograms was partitioned in equal zones (Fig. 6, panel A1-B1). A pink color progressively changing to white was used to identify the scaffold whereas a red color turning to cyan was applied to the new bone phase. Additionally, the green-cyan colors were chosen to identify the transition phase. In Fig. 6 (panel A-B) two different 3D-reconstructions of the same volume and their partitioned histograms for the 16 weeks implant are shown. The segregation of the pink hues close to the bone deposition zones, which characterizes the scaffold phase observed in

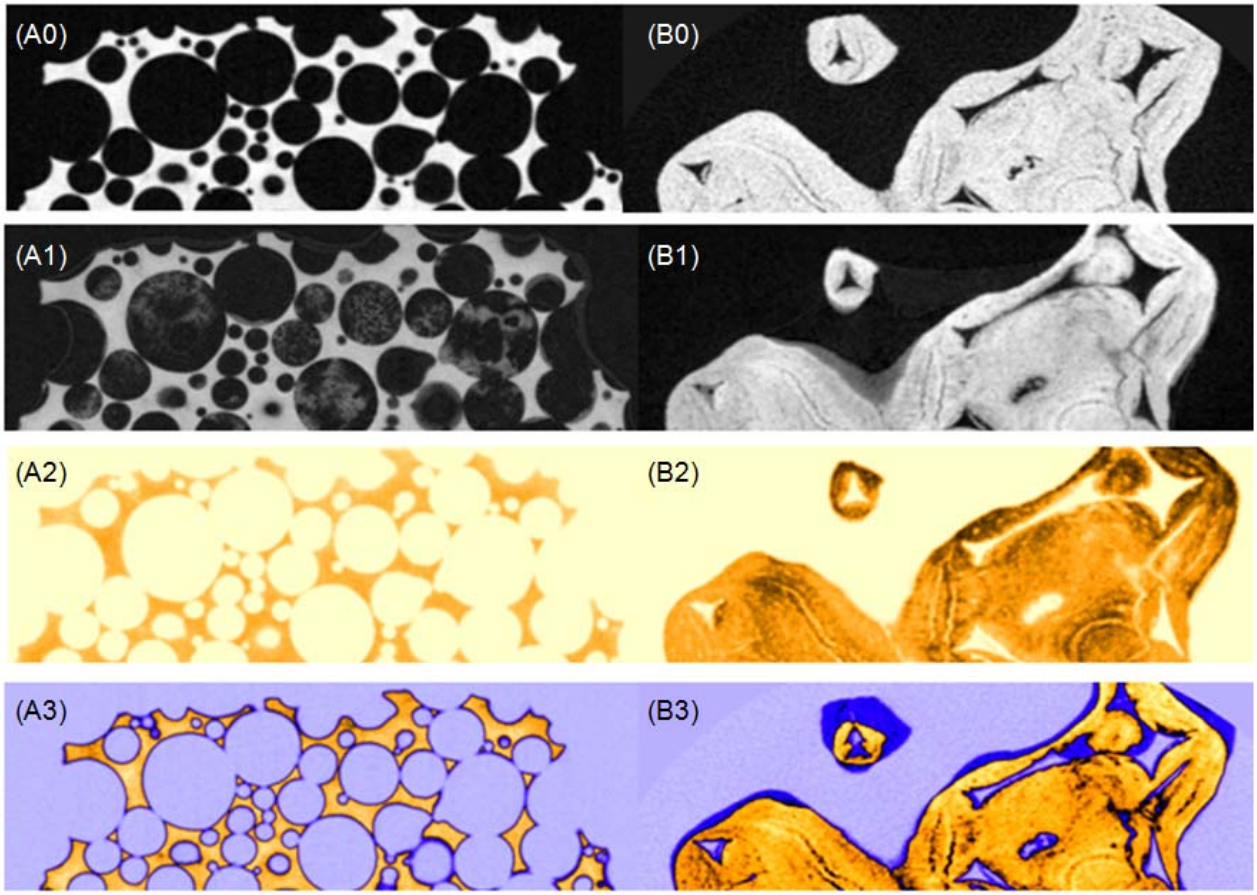

Fig. 3: 2D original slices of scaffolds before and after implantation: **(A)** Engipore and B) Skelite™. Slices of implanted samples before **(A0-B0)** and after 8 weeks **(A1-B1)** implantation. In the panels A2-B2 are presented the segmented images after implantation (scaffold – yellow). In the panels **A3-B3** are presented the images obtained by combining the data of panels **A0-B0** with those of panels **A2-B2**. Blue volumes indicate portions of scaffolds present in panels **A0-C0** (pre-implant).

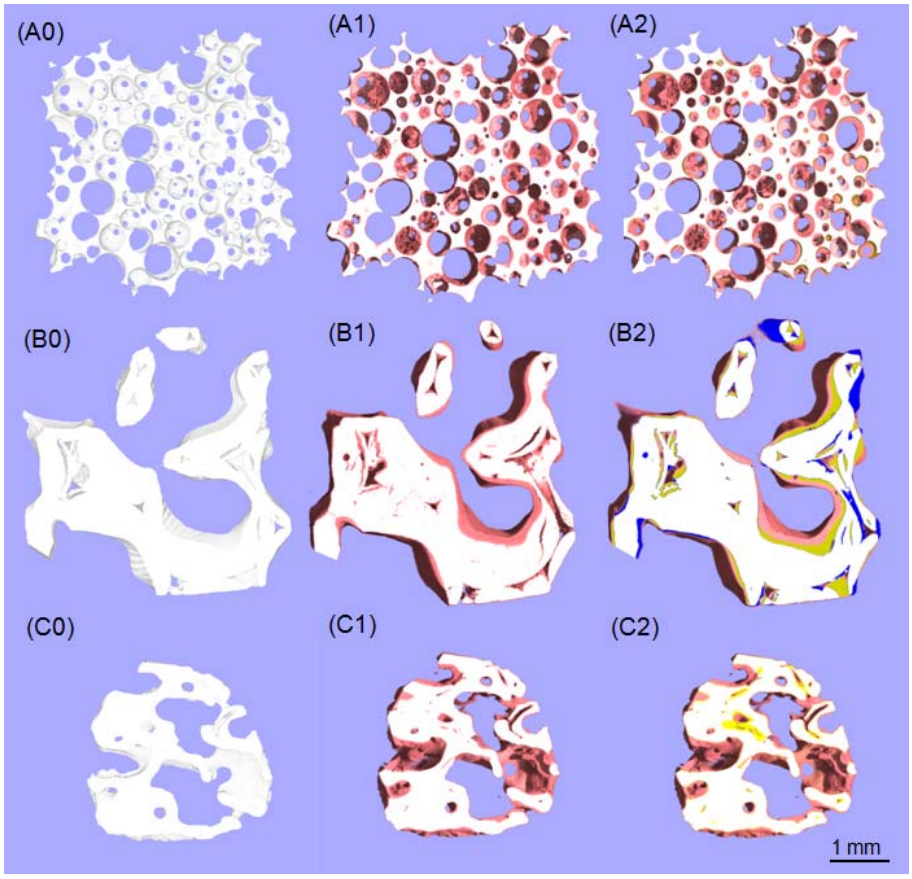

Fig. 4: 3D display of sub-volumes of scaffolds before and after implantation: **(A)** Engipore; **(B)** Skelite™; **(C)** Bio-Oss®; **(A1-C1)** Sub-volumes of implanted samples before **(A0-C0)** and after 8 weeks **(A1-C1)** implantation. The images show the new bone (pink) on the surface of the scaffolds (white). In the panels **A2-C2** are presented the images obtained by combining (registering) the data of panels **A0-C0** with those of panels **A1-C1**. Blue volumes indicate portions of scaffolds present in panels **A0-C0** (pre-implant) and absent in panels **A1-C1** (after implantation) and correspond to completely resorbed scaffold. Yellow volumes indicate virgin scaffold volume in which after implantation a reduction of the sample density is observed (see text).

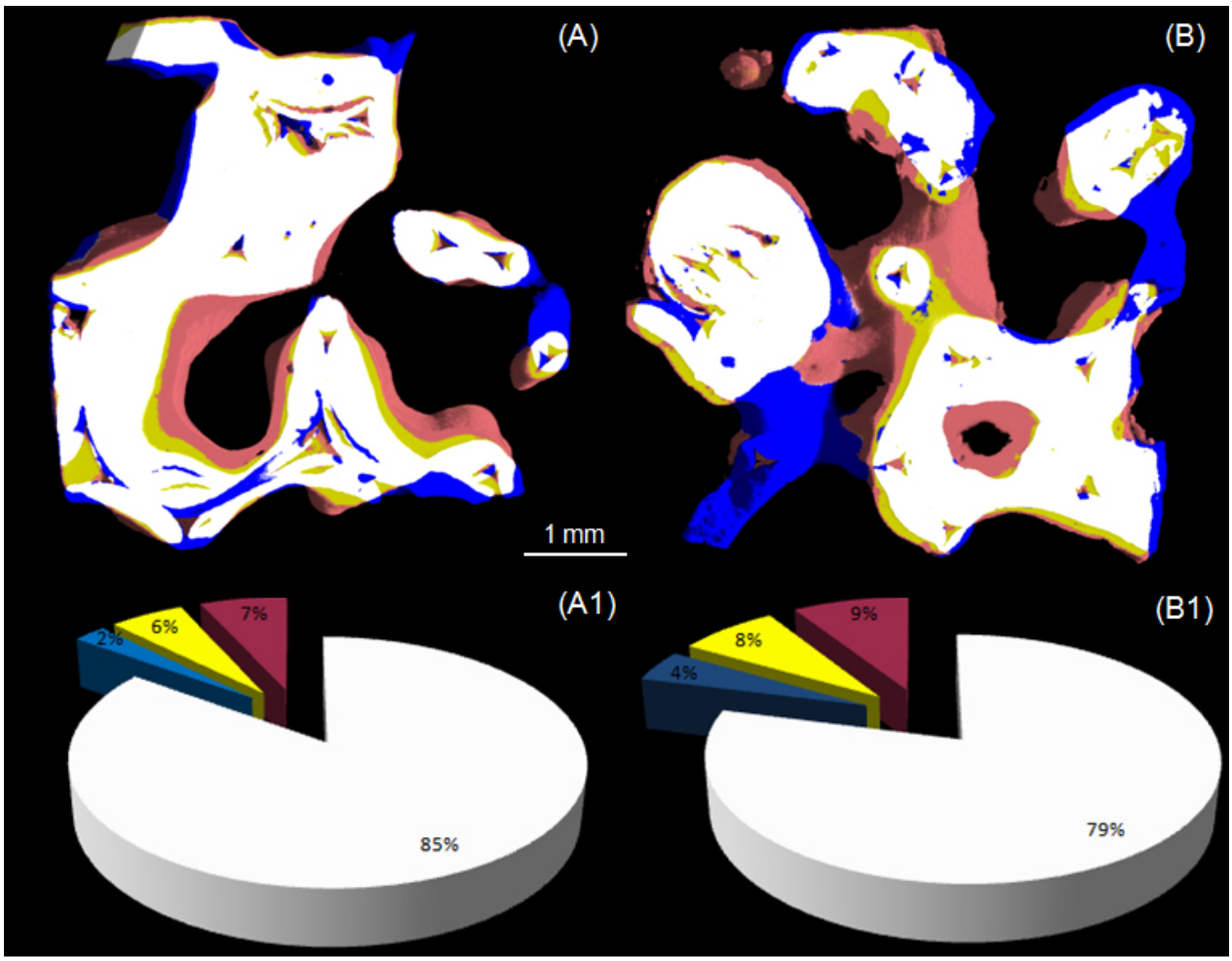

Fig. 5: Display based on a combination of the 3D structure of pre- and post implanted Skelite™ samples for 8 **(A)** and 16 **(B)** weeks, respectively (white – scaffold; pink – new bone; blue – total resorption; yellow – partial resorption (see caption of Fig. 3). **(A1-B1)** volume percentage distribution of the different phases.

Table 2. Histomorphometric data for MSC seeded scaffolds after 8 week implantation

	NB.Th (microns)	NB.V (%)	S.Th (microns)
Engipore	34±5	5.2±0.5	99±41
Skelite™	47±5	7.1±0.5	134±123
Bio-Oss®	53±5	8.4±0.5	131±45

NB.Th = newly formed bone mean thickness; NB.V = newly formed bone volume; S.Th = scaffold mean thickness after implantation.

the post-implant scaffolds (panel A-B), but not in the pre-implant scaffold (not shown), suggests that the new bone deposition was associated with the occurrence of some scaffold alterations.

For the same sample sub-volume a registration was performed of the scaffolds before and after implantation (panels C-F). Panel F is a replica of panel D in which the blue volumes (completely resorbed scaffold) have been canceled and the red volume (bone) made transparent to better visualize the volumes underneath. Arrowheads indicate some of the areas of resorbed scaffold where new bone has been deposited (Compare panel F and panel A).

To complete the study, composition and volumes of the Skelite™ scaffolds and new bone volumes were quantified in samples implanted for different times, from 3 days to 24 weeks. Volume histograms of implanted scaffolds are shown in Fig. 6A. In the pre-implanted Skelite™ scaffolds 2 peaks were observed for relatively high values of the coefficient, corresponding to the scaffold material two components – tricalcium phosphate (TCP) and hydroxyapatite (HA). The TCP volume decreased with increasing time of implantation. The HA volume was almost constant. In the implanted samples for more than 2 weeks an additional peak was observed at lower X-ray

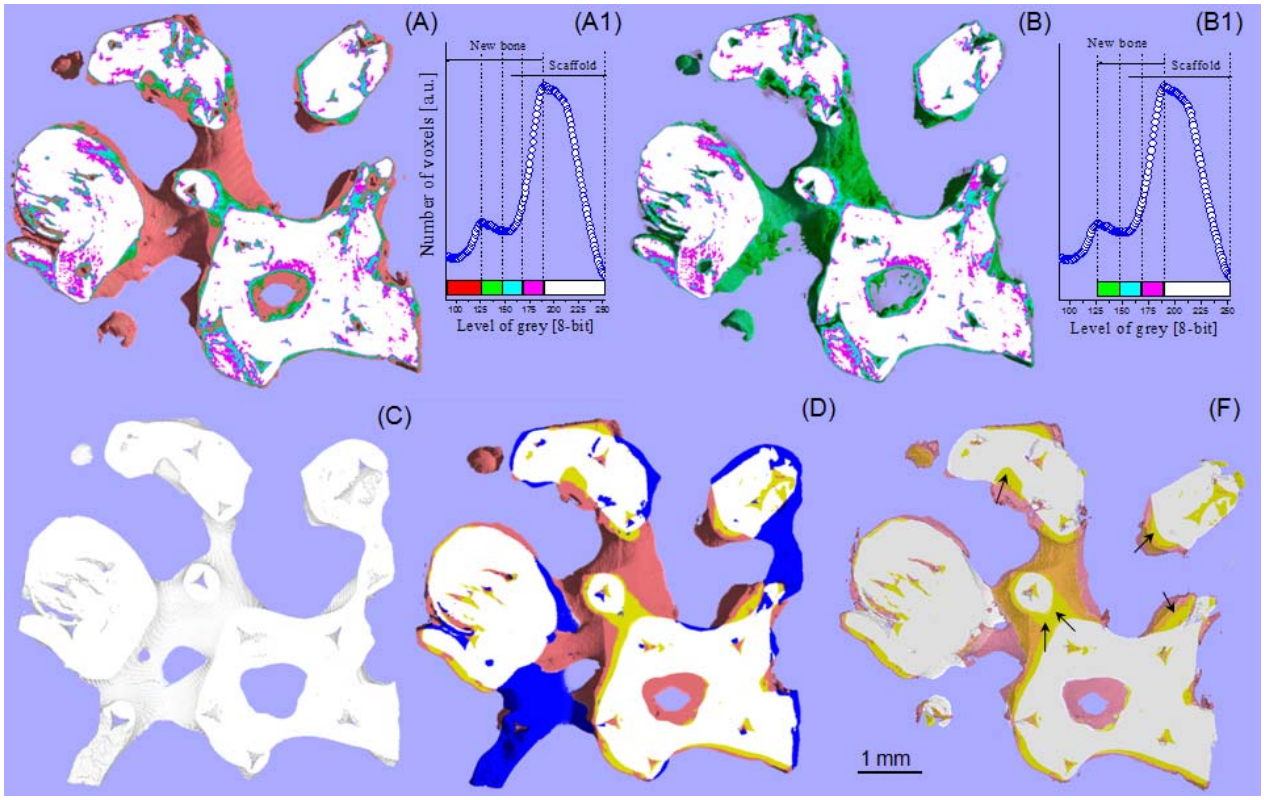

Fig. 6: (A-B) 3D display of a random segmented sub-volume of Skelite™ after 16 weeks implant. Color based segmentation was performed according to volume histogram in Panel A1-B1; **(C)** 3D display of the same subvolume of the SkeliteTM scaffolds before implant; **(D)** 3D displays of registered pre- and post-implanted samples. White – scaffold, pink – new bone, blue – total resorption, yellow – partial resorption (see caption of Fig. 3); **(E)** The same 3D display where resorbtion (blue) is cancelled and the new bone is transparent.

absorption values corresponding to the new bone. It can be seen that the central position of this peak associated with the new bone shifts to higher values, as far as the implantation time is increased. This effect is attributed to the progressive increase of the degree of mineral concentration (inducing an increase in the linear absorption coefficient) as a function of implantation time. Histomorphometric data for scaffolds after implantation are reported in Table 2.

Discussion

An ideal scaffold for bone tissue engineering should initially provide a support for the bone deposition by the osteogenic cells, and then it should be resorbed at a rate corresponding to the one of bone formation upon replacement of the scaffold by the new bone tissue. Ceramic scaffolds made of TCP or HA/TCP have been extensively used in bone tissue engineering. TCP is the main resorbable component of such scaffolds. However, TCP is resorbed by random dissolution, while the ideal scaffold should be resorbed by cell-mediated processes, contemporary to the new bone deposition.

We previously reported evidence for a coupling between bone formation and scaffold biodegradation when ceramic scaffolds based on silicon stabilized tricalcium phosphate (Si-TCP; Skelite™), seeded with bone marrow derived mesenchymal stem cells were ectopically implanted for 2, 4 and 6 months in immunodeficient mice (Papadimitropoulos *et al.*, 2007). When we analysed the implanted scaffolds by X-ray synchrotron radiation microCT, the experimental approach allowed the extraction of several structural and morphometric parameters and the kinetics of the tissue engineered bone growth in connection with the biodegradation rate of the scaffold. Simultaneous investigation on 100% HA was presented too, where, as expected, no scaffold resorption was observed.

In the present work that should be considered a continuation and an implementation of the previous one, in addition to 100% HA and Si-TCP, also a natural bone mineral derived scaffold (Bio-Oss®) was investigated, using X-ray synchrotron radiation microCT. The seeding with MSC and the implantation in the immunodeficient mice were performed according to the same protocol as used previously (Papadimitropoulos *et al.*, 2007); the implantation times for all three different scaffolds were 8 and 16 weeks, respectively. On the contrary, a significant improvement was introduced in the imaging procedure, by making possible the comparison of the same subvolumes of the samples before and after implantation as will be discussed below. In addition, a detailed kinetic study was performed for Skelite™ scaffolds implanted for times that varied between 3 days and 24 weeks.

The images of the three scaffolds before implantation revealed an appreciable difference among their morphologies (Fig. 1). In particular the Bio-Oss®, which was investigated by us for the first time, contained elongated ellipsoidal pores, whereas the HA scaffold contained roughly spherical pores.

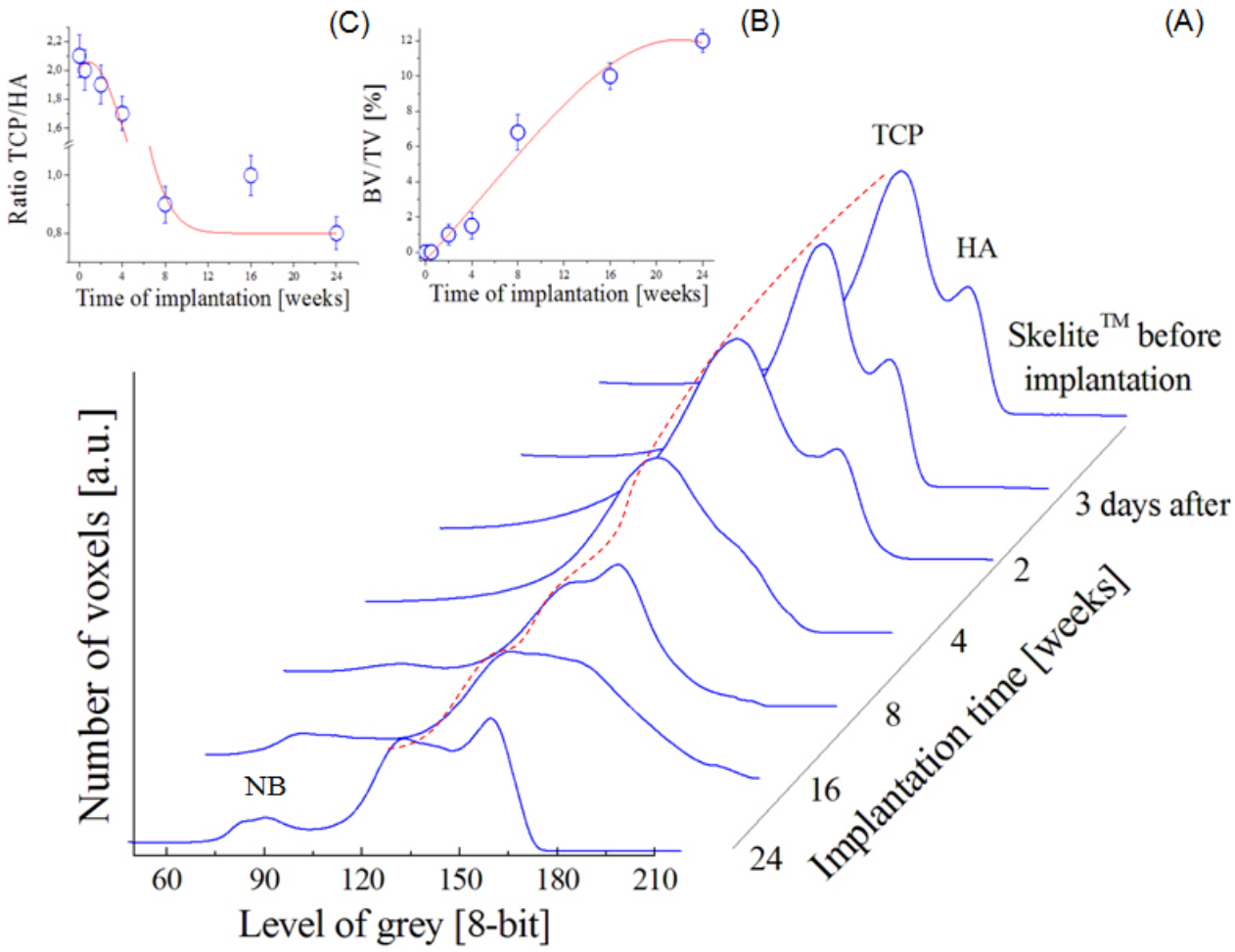

Fig. 7: Volume histograms of SkeliteTM scaffolds implanted from 3 days to 24 weeks (NB – new bone, TCP – tricalcium phosphate, HA – hydroxyapatite). **(A)** New bone deposition kinetics; **(B)** Percentage of bone volume/ total volume; **(C)** TCP/HA mean ratio as a function of the implantation time.

The histograms of the distribution of the thickness of the scaffold wall of Fig. 2 (A) and 2(B), confirmed the results previously obtained in (Papadimitropoulos *et al.*, 2007), namely biodegradation for the Si-TCP scaffold and lack of it for the HA scaffold. The newly investigated Bio-Oss® showed a very little decrease of the scaffold wall thickness; the decrease was at the limit of detectability, and needs to be confirmed by additional experiments. Panels A1-C1, obtained by an imaging technique, not used in (Papadimitropoulos *et al.*, 2007), give an instantaneous pictorial view of the variation in scaffold wall thickness and confirm in a rather impressive way the uniqueness of the biodegradation process in Skelite™.

Probably the strongest driver for combined imaging in bone tissue engineering is its capability to provide an appreciable contribution to a better understanding of the scaffold biodegradation phenomenon. The obtained results demonstrated the benefits of the imaging treatment used in the present study. However, a registration algorithm that has been configured for a specific target application such as a scaffold biodegradation study must be validated in view of the application requirements. Validation requires some basic truth from which the quality of a registration result can be inferred (Hamisch *et al.*, 2006). Therefore, some phantom images are needed which can provide a basic truth for a technical validation to estimate consistency and accuracy of a registration procedures. In our case the study was performed on Engipore scaffold in order to obtain a validation of the registration used. We showed that Engipore scaffold before and after implantation were superimposed with a high accuracy. This result correlates with the common knowledge based on literature data that HA is a non-biodegradable material. Moreover, the observed and quantified general biodegradation behavior of Skelite™ and Bio-Oss® according to the present work were in agreement with previously reported data (Komlev *et al.*, 2006; Cancedda *et al.*, 2007; Merkx *et al.*, 1997; Merkx *et al.*, 1999; Rumpel *et al.*, 2006).

On this basis, to obtain information on the 3D structural changes of the scaffolds occurring during the implantation, the same image treatment that allows a direct comparison of the 3D structure (before and after implantation) of the same sub-volume of a given scaffold, was applied to all three scaffolds. The data reported in Figures 4-6 show the good performance of the adopted procedure, demonstrating the visualization at the same time of both the tissue-engineered bone growth and the complete or partial biodegradation of the scaffold.

The analysis proposed in the present paper is a major improvement as compared to the imaging procedure adopted in our previous work (Papadimitropoulos *et al.*, 2007), where only a comparison between different sub-

volumes of the implants before and after implantation was made.

Finally, a high content of innovation is associated to the detailed kinetics studies on the Skelite™ scaffolds implanted for different times, not only due to the large number of the implantation times investigated, but also to the recording in the X-ray absorption histograms of separate peaks associated to HA and TCP in the same scaffold (Fig. 7). It is therefore possible to observe that the progressive biodegradation of Skelite™ scaffold is eventually due to the TCP component.

It should be noted that when we investigated by micro-diffraction studies the interfaces between the newly formed bone and the Skelite™ scaffold, the local structural study at the interface indicated that scaffold biodegradation was mainly due to TCP depletion (Papadimitropoulos *et al.*, 2007).

Moreover, saturation in the TCP resorption occurred at an implantation time of about 8 weeks, whereas saturation in the tissue engineered bone occurred at an implantation time of about 24 weeks. This could indicate that the bone growth did not occur only in the scaffold volume that was resorbed, but also in the inward direction with respect to the pore surface. This finding is in agreement with the results presented in Fig. 5 of reference (Mastrogiacomo *et al.*, 2007), and in Fig. 4 of reference (Papadimitropoulos *et al.*, 2007).

Conclusion

The obtained results in addition to confirming the well-known non-biodegradability of HA demonstrated that the observed and quantified general biodegradation behavior of Skelite™ and Bio-Oss® is in agreement with that reported in (Komlev *et al.*, 2006; Cancedda *et al.*, 2007; Merkx *et al.*, 1997; Merkx *et al.*, 1999; Rumpel *et al.*, 2006).

Nevertheless, the promising and effective 3D microCT registration procedure employed in the present work, together with the adoption of a large number of implantation times, introduces an appreciable increase in the existing information with regard to biodegradation of bone mimetic scaffolds and of Si-TCP based scaffolds in particular. The new approach allows a deeper insight in the investigated biological phenomena, and can be extrapolated further in bone tissue engineering research possibly by combining the data with the 3D data on angiogenesis obtained by the use of holotomographic technique (Komlev *et al.*, 2009).

Acknowledgements

Supported by funds from the Italian (ASI) and the European (ESA-ERISTO) Space Agencies and from FP7 EU (Angioscaff) funds.

References

Anselme K, Noël B, Flautre D, Blary M-C, Delecourt C, Descamps M, Hardouin P (1999) Association of porous hydroxyapatite and bone marrow cells for bone regeneration. Bone **25**: 51S-54S.

Brown L (1992) A survey of image registration techniques. ACM Comp Surv **24**: 325-376.

Bumgardner JD, Vasquez-Lee M, Fulzele KS, Smith DH, Branch KD, Christian SI, Williams DH (2004) Biocompatibility Testing. In: Encyclopedia of Biomaterials and Biomedical Engineering, Marcel Dekker, New York, pp 79-88.

Cancedda R, Cedola A, Giuliani A, Komlev V, Lagomarsino S, Mastrogiacomo M, Peyrin F, Rustichelli F (2007) Bulk and interface investigations of scaffolds and tissue-engineered bones by X-ray microtomography and X-ray microdiffraction. Biomaterials **28**: 2505-2524.

Cancedda R, Dozin B, Giannoni P, Quarto R (2003) Tissue engineering and cell therapy of cartilage and bone. Matrix Biol **22**: 81-91.

Dougherty RP, Kunzelmann K-H (2007) Computing local thickness of 3D structures. Microsc Microanal **13**(Suppl 2): 1678CD.

Duda M, Pajak J (2004) The issue of bioresorption of the Bio-Oss xenogeneic bone substitute in bone defects. Ann Univ Mariae Curie Sklodowska [Med] **59**: 269-277.

Giannoni P, Mastrogiacomo M, Alini M, Pearce SG, Corsi A, Santolini F, Muraglia A, Bianco P, Cancedda R (2008) Regeneration of large bone defects in sheep using bone marrow stromal cells. J Tissue Eng Regen Med **2**: 253-262.

Hamisch Y, Egger M, Hines H, Fiedler K, Carlsen I (2006) Clinical hybrid imaging: image co-registration and hardware combination for PET/CT and SPECT/CT. In: Advances in Healthcare Technology (Spekowius G, Wendler T, eds), Springer, Dordrecht, The Netherlands, pp 117-138.

Hench LL, Polak JM (2002) Third-generation biomedical materials. Science **295**: 1014-1017.

Iyer S, Sinha SK (2006) Segmentation of pipe images for crack detection in buried sewers. Computer-Aided Civil and Infrastructure Engineering **21**: 395-410.

Klinck J, Boyd SK (2008) The magnitude and rate of bone loss in ovariectomized mice differs among inbred strains as determined by longitudinal *in vivo* micro-computed tomography. Calcif Tissue Int **83**:70-79.

Knabe C, Koch Ch, Rack A, Stiller M (2008) Effect of β-tricalcium phosphate particles with varying porosity on osteogenesis after sinus floor augmentation in humans. Biomaterials **29**: 2249-2258.

Komlev VS, Mastrogiacomo M, Peyrin F, Cancedda R, Rustichelli F (2009) X-ray synchrotron radiation pseudo-holotomography as a new imaging technique to investigate angio- and microvasculogenesis with no usage of contrast agents. Tissue Eng **15**: 425-430.

Komlev VS, Peyrin F, Mastrogiacomo M, Cedola A, Papadimitropoulos A, Rustichelli F, Cancedda R (2006) Kinetics of *in vivo* bone deposition by bone marrow stromal cells into porous calcium phosphate scaffolds: an X-ray computed microtomography study. Tissue Eng **12**: 3449-3458.

Langer R, Vacanti JP (1993) Tissue engineering. Science **260**: 920-926.

Mastrogiacomo M, Papadimitropoulos A, Cedola A, Peyrin F, Giannoni P, Pearce SG, Alini M, Giannini C, Guagliardi A, Cancedda R (2007) Engineering of bone using bone marrow stromal cells and a silicon-stabilized tricalcium phosphate bioceramic. Evidence for a coupling between bone formation and scaffold resorption. Biomaterials **28**: 1376.

Matheron G (1975) Random sets and integral geometry. Wiley, New York.

Merkx MA, Maltha JC, Freihofer HP,Kuipers-Jagtman AM (1999) Incorporation of three types of bone block implants in the facial skeleton. Biomaterials **20**: 639-645.

Merkx MA, Maltha JC, van't Hoff M, Kuijpers-Jagtman AM, Freihofer HP (1997) Tooth eruption through autogenous and xenogenous bone transplants: a histological and radiographic evaluation in beagle dogs. J Craniomaxillofac Surg **25**: 212-219.

Modersitzki J (2004) Numerical Methods for Image Registration. Oxford University Press.

Muraglia A, Martin I, Cancedda R, Quarto R (1998) A nude mouse model for human bone formation in unloaded conditions. Bone **22**: 131S.

Otsu N (1979) A threshold selection method from gray-level histograms. IEEE Trans Syst Man Cybernet SMC-**9**: 62-66.

Papadimitropoulos A, Mastrogiacomo M, Peyrin F, Molinari E, Komlev VS, Rustichelli F, Cancedda R (2007) Kinetics of *in vivo* bone deposition by bone marrow stromal cells within a resorbable porous calcium phosphate scaffold: an X-ray computed microtomography study Biotech Bioengin **98**: 271-281.

Peyrin F, Mastrogiacomo M, Cancedda R, Martinetti R (2007) SEM and 3D synchrotron radiation micro-tomography in the study of bioceramic scaffolds for tissue-engineering applications. Biotech Bioengin **97**: 638-648.

Renghini C, Komlev V, Fabrizio F, Verne E, Baiono F, Vitale-Brovarone C (2009) Micro-CT studies on 3-D bioactive glass-ceramics scaffolds for bone regeneration. Acta Biomater **5**: 1328-1337.

Rumpel E, Wolf E, Kauschke E, Bienengräber V, Bayerlein T, Gedrange T, Proff P (2006) The biodegradation of hydroxyapatite bone graft substitutes *in vivo*. Folia Morphol **65**: 43-48.

Salome M, Peyrin F, Cloetens P, Odet C, Laval-Jeantet AM, Baruchel J, Spanne P (1999) A synchrotron radiation microtomography system for the analysis of trabecular bone samples. Med Phys **26**: 2194.

Schenk RK (1991) Zur Problematik der Knochenersatzstoffe: Histophysiologie des Knochenumbaus und der Substitution von Knochenersatzstoffen. (The problems of bone replacement materials. Histophysiology of bone remodeling and the substitution of bone replacement materials). In: Huggler AH, Kuner EH (eds.) Hefte Unfallheilkd. **216**: 23-35.

Schepers E, Declercq M, Ducheyne P, Kempeneers R (1991) Bioactive glass particulate material as a filler for bone lesions. J Oral Rehab 18: 439-52.

Schmitt O, Modersitzki J, Heldmann S, Wirtz S, Fischer B (2007) Image registration of sectioned brains. Inter J Comp Vision **73**: 5-39.

Sánchez Sorzano CÓ, Thévenaz P, Unser M (2005) Elastic registration of biological images using vector-spline regularization. IEEE Trans Biomed Eng **52**: 652-663.

Serra J (1982) Image analysis and mathematical morphology. Academic Press, London.

Stokking R, Zubal IG, Viergever MA (2003) Display of fused images: methods, interpretation, and diagnostic improvements. Semin Nucl Med **33**:219-227.

Suba Z, Takacs D, Matusovits D, Barabas J, Fazekas A, Szabo G (2006) Maxillary sinus floor grafting with β-tricalcium phosphate in humans: density and microarchitecture of the newly formed bone. Clin Oral Implants Res **17**: 102-108.

Tadjoedin ES, de Lange GL, Holzmann PJ, Kulper L, Burger EH (2000) Histological observations on biopsies harvested following sinus floor elevation using a bioactive glass material of narrow size range. Clin Oral Implants Res **11**: 334-344.

van den Elsen P, Pol E-J, Viergever M (1993) Medical image matching – a review with classification. IEEE Eng Med Biol **12**:26-39.

Waarsing JH, Day JS, Verhaar JA, Ederveen AG, Weinans H (2006) Bone loss dynamics result in trabecular alignment in aging and ovariectomized rats. J Orthop Res **24**: 926-935.

Zaffe D, Leghissa GC, Pradelli J, Botticelli AR (2005) Histological study on sinus lift grafting by Fisiograft and Bio-Oss. J Mat Sci Mat Med **16**: 789-793.

Discussion with Reviewer

Reviewer I: Presumably the registration process would have minimized the occurrence of implant material in regions where it did not exist before implantation. Were there any exceptions?

Authors: Of course, there are some exceptions and uncertainness. The occurrence of implant material in regions where it did not exist before implantation can appear as a biodegradable phase. Future studies could minimize some exceptions by developing appropriate algorithms.

Reviewer I: Was the implant resorption fairly uniform, or were there localized regions of high absorption?

Authors: The biodegradation of scaffolds took place mainly in the area of new bone growth. In the absence of new bone, the resorption is minor and fairly uniform.

Reviewer I: Was there any evidence of fragmentation of the implant or just a thinning of the walls?

Authors: Generally, thinning of the walls was observed. However, there was some evidence of fragmentation of the scaffolds (data not shown).